On the Selection of Limiting Hydrodynamic Conditions for the Supercritical AntiSolvent (SAS) Process

Alvaro Tenorio,*,† Philip Jaeger,‡ Maria D. Gordillo,† Clara M. Pereyra,† and Enrique J. Martínez de la Ossa†

Department of Chemical Engineering, Food Technology and Environmental Technologies, Faculty of Sciences, University of Cádiz, 11510 Puerto Real (Cádiz), Spain, and Thermal and Separation Process, Technische Universität Hamburg−Harburg, Eissendorfer Strasse 38 (O), D-21073 Hamburg, Germany

The Supercritical AntiSolvent (SAS) technique (which is also referred to as ASES, PCA, or SEDS in the literature) is a promising means of overcoming the low bioavailability found in some active pharmaceutical compounds (APIs). By determining the thermodynamic properties of the phases involved in the process, and applying empirical equations (operations with dimensionless numbers), it has been possible to estimate the different disintegration regimes of the jet when an *N*-methyl-pyrrolidone (NMP)−ampicillin solution is injected into the CO_2-pressurized chamber under pressure (P), temperature (T), and flow rate (Q_L) conditions in the following ranges: $P = 80-180$ bar, $T = 308-328$ K, $Q_L = 1-5$ mL/min. The application of the empirical hydrodynamics model highlights the existence of significant mechanisms that stabilize the liquid jet, and it shows that there are limiting hydrodynamic conditions that must be overcome to direct the process toward the formation of uniform spherical nanoparticles and the achievement of higher yields.

1. Introduction

The production of monodisperse microparticles and nanoparticles of active ingredients by means of the Supercritical AntiSolvent (SAS) technique has been under investigation for many applications during the last 10 years. This reduction in particle size to microscale and/or nanoscale represents considerable value added for those drugs whose application requires this size range for increased therapeutic efficacy. The reduction in size of active pharmaceutical compounds, along with the production of particles of quite uniform size, is sought especially, to optimize their bioavailability.[1−3]

In the SAS process, the disperse phase is formed by the solute to be micrometerized dissolved in an organic solvent; the continuous phase comprises the supercritical phase, in such a way that the organic solvent and the supercritical phase must be partial (below the critical point of the mixture, MCP) or completely miscible (above the MCP), under the operating conditions of the process. The solution is dispersed in the fluid at high pressure by nebulizers or capillaries with orifice diameters of the order of hundreds of micrometers, generating sufficient contact area between the phases to increase the transfer of matter in the two directions; that is, the solvent diffuses into the supercritical fluid (evaporation) and this diffuses into the liquid phase, generating an antisolvent effect (supersaturation) that causes the precipitation of the solute. When dealing with pharmaceutical products, supercritical carbon dioxide (SC CO_2) is the most widely used solvent in the SAS processes.

The way in which the liquid solution is dispersed in the CO_2 at high pressure is dependent on whether the operating pressure is above or below the MCP at the operating temperature used. When the operating conditions are below the MCP, it disintegrates (rather like the disintegration of a liquid jet at atmospheric pressure), which is strongly influenced by the operating pressure and the flow rate of liquid solution, according to one of the following three regimes: the Rayleigh breakup regime, which is characterized by a rupture of the jet in the form of monodisperse droplets; the sine wave breakup regime, in which a helicoidal oscillation of the jet occurs, leading to its rupture into droplets with a polydisperse distribution; and atomization, in which the jet is smooth when it leaves the orifice, until it reaches the zone of highly chaotic rupture where a cone of atomized liquid is formed. Above the MCP, it is not possible to distinguish separate entities (droplets) nor interfaces between the liquid solution and the phase of dense CO_2 gas; consequently, the flow regime would be similar to that of a gaslike jet and will be characterized by the degree of turbulence associated with the vortices produced in the solvent medium: SC CO_2.

Therefore, the technical viability of the SAS process requires knowledge of (a) the phase equilibrium existing into the system; (b) the hydrodynamics: the disintegration regimes of the jet; (c) the kinetics of the mass transfer between the dispersed and the continuous phase; and (d) the mechanisms and kinetics of nucleation and crystal growth. With only some exception,[4−6] in the models developed for the SAS process, the hydrodynamics step received only limited consideration. This is in contrast with the fact that hydrodynamics is an important step for the success or the failure of the entire process. For these reasons, the present study is focused on the investigation of the disintegration regime of the liquid jet into the SC CO_2. In particular, the objective of the present study is to establish a correlation between the morphologies of the particles obtained in the ampicillin precipitation assays and the regimes estimated; this correlation will enable the limiting hydrodynamic conditions for the success of the test to be defined; that is, the appropriate conditions to orientate the process toward the formation of uniform spherical nanoparticles instead of irregular and larger-sized particles, for the solute−solvent−SC CO_2 system studied.

* To whom correspondence should be addressed. Tel.: +34-956-016-458. Fax: +34-956-016-411. E-mail: alvaro.tenorio@uca.es.

† Department of Chemical Engineering, Food Technology and Environmental Technologies, Faculty of Sciences, University of Cádiz.

‡ Thermal and Separation Process, Technische Universität Hamburg−Harburg.

10.1021/ie801940p CCC: $40.75 © 2009 American Chemical Society
Published on Web 09/04/2009

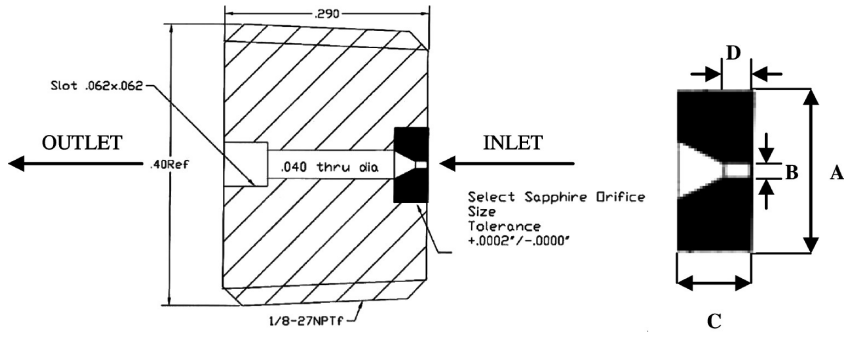

Figure 1. Schematic diagram of the nebulizer utilized with a sapphire plate; outside diameter = 2210 μm. Legend: inside diameter (B) = 100 or 200 μm; thickness (C) = 1194 μm; and length of hole (D) = 254 μm.

2. Experimental Section

The present article reports a study that was conducted on the hydrodynamics in a series of experiments for ampicillin precipitation by the SAS technique, utilizing *N*-methyl-pyrrolidone (NMP) as the solvent and CO_2 as the antisolvent, under pressure (P), temperature (T), and flow rate (Q_L) conditions in the following ranges: $P = 80-180$ bar, $T = 308-328$ K, $Q_L = 1-5$ mL/min.[7,8]

By determining the thermodynamic properties of the phases involved in the process, and applying empirical equations (operations with dimensionless numbers),[9] it will be possible to estimate the different disintegration regimes of the jet when the solution of NMP is injected into the pressurized chamber by means of two nebulizers, with orifice diameters ($Ø_n$) of 100 and 200 μm, respectively, under different operating conditions.

2.1. Materials and Experimental Setup for the SAS Process. 1-Methyl-2-pyrrolidone (NMP) (99.5% purity) was purchased from Sigma−Aldrich Chemical (Spain), and carbon dioxide with a minimum purity of 99.8% was supplied by Carburos Metálicos S.A. (Spain).

The equipment used to perform the experiments was developed by Thar Technologies (SAS 200 model). The SAS 200 system was comprised of the following components: two high-pressure pumps, one for the CO_2 and the other for the solution; a stainless steel precipitator vessel with a volume capacity of 2 L, consisting of two parts (the main body and the frit); an automated back-pressure regulator of high precision; and a stainless steel cyclone separator with a volume capacity of 0.5 L. More equipment details and operating procedures have been given elsewhere.[8]

From the point of view of the hydrodynamics of the process, it is important to consider the design of the nebulizers utilized in the present study. As can be seen in Figure 1, these are formed by a stainless steel body that acts as a support element for a sapphire plate containing orifices with diameters of 100 and 200 μm, through which the liquid is injected into the high-pressure chamber.

Because the orifice operates at very high pressures in our system, the sapphire plate is mounted on the support of stainless steel in such a way that the flow of liquid first passes through the orifice and emerges as a jet from the conical zone of the device. In this way, the plate−support assembly will have greater mechanical strength, and it will be able to operate at higher flow rates, because the coefficient of discharge (C_d) of the conical zone is greater than that of the orifice in the wall.

2.2. Experimental Setup and Procedure for Measurement of the Interfacial Tension. The pendant droplet method, as introduced by Andreas and Hauser,[10] was used in this work to determine the interfacial tension between NMP and SC CO_2.

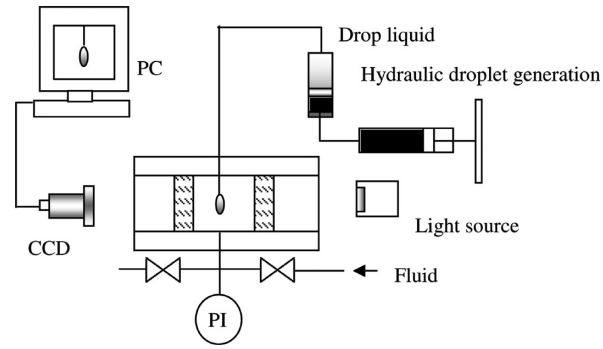

Figure 2. Experimental setup with a viewing chamber and liquid/fluid metering system.

This method, and its application to high pressures and temperatures, are comprehensively described by Eggers and Jaeger.[11] From the shape and dimensions of a liquid droplet hanging at a capillary tip, which is surrounded by a second (transparent) fluid, the interfacial tension can be determined if the density difference between the two coexisting fluids is known.[12] A commercial CCD video technique allows recording of droplet shapes for subsequent video image processing. A schematic diagram of the experimental setup for pendant droplet measurements used in this work is shown in Figure 2. The principle of the measurement is briefly described below.

The viewing chamber is thermostatted to the desired temperature before the chamber is filled with CO_2 to the designated pressure. After allowing sufficient time for thermal equilibration, droplets of NMP are generated at the capillary tip using a manual syringe pump. As soon as a mechanically stable droplet is obtained, video recording is started. In any case, for common organic liquids in combination with CO_2, only negligible effects of the age of the droplet have been detected so far.

After the droplet shape is digitalized, a calculation procedure is started, to modify the value of the interfacial tension until the theoretical droplet profile fits the experimental shape perfectly. The result is the value of the interfacial tension between the two fluids at the given temperature and pressure. Some examples of droplet images are depicted in Figure 3.

3. Empirical Model Application

3.1. Theory. Rayleigh breakup, sinusoidal wave breakup, and atomization regimes are seen to be clearly differentiated by representing graphically the Reynolds number (Re_L) against a dimensionless number Z, formed by the Weber number (We_L) and Re_L; this number was later named the Ohnesorge number (Oh). Here, the forces of inertia of the liquid phase (pressure gradient), the forces of capillarity (surface tension), and those

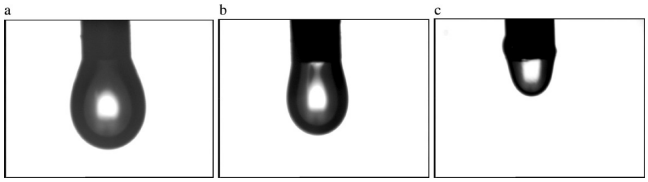

Figure 3. Droplets of NMP in CO_2 at $T = 55$ °C and (a) $P = 1$ bar, (b) $P = 40$ bar, and (c) $P = 100$ bar.

of viscosity of the liquid phase (friction) are taken into account, but the force of gravity is considered to be negligible.

With increases in the operating pressure, and therefore, with increases in the density of the gaseous phase, the aerodynamic forces begin to be important, and the regime limits previously stated are moved toward lower Re_L values. Lefebvre[13] demonstrated the relevance of these aerodynamic forces (the We_g value of the gaseous phase) during the process of disintegration of the jet in a high-pressure chamber; moreover, to take this influence into account, Czerwonatis and Eggers[9] considered a new dimensionless number, Z^*, which is the result of multiplying the Ohnesorge number (Oh) by the square root of the Weber number of the gas phase ($(We_g)^{1/2}$):

$$Z^* = Oh_l\sqrt{We_g} = \frac{\eta_l v}{\sigma}\sqrt{\frac{\rho_g}{\rho_l}} \quad (1)$$

By representing the Z^* numbers vs Re_L graphically, it was possible to determine the limits that describe the disintegration of the liquid stream in the presence of CO_2 at high pressure. However, additional experiments of Czerwonatis and Eggers[9] revealed that the viscosity of the gaseous phase is also important; that is, an increased viscosity of the gas produces a more powerful cutting effect on the external surface of the jet, thus destabilizing it to a greater extent. This effect was considered by introducing a dimensionless number Z^{**}, which is the result of multiplying Z^* by the square root of the quotient of viscosities of the gas and liquid phases:

$$Z^{**} = Z^*\sqrt{\frac{\eta_l}{\eta_g}} = \frac{\eta_l v}{\sigma}\sqrt{\frac{\rho_g}{\rho_l}}\sqrt{\frac{\eta_l}{\eta_g}} \quad (2)$$

The representation of Z^{**} vs Re_L finally allowed the limits of disintegration of the liquid stream in CO_2 at high pressure to be determined in a single graph, giving rise to the following empirical equations:

boundary between Rayleigh and sine wave breakup:

$$Z^{**} = 10^{3.9}Re^{-1.66} \quad (3)$$

boundary between sine wave breakup and atomization:

$$Z^{**} = 10^{5}Re^{-1.73} \quad (4)$$

3.1.1. Critical Jet Velocity. Especially important in the SAS process is the critical velocity of the jet, because the finer the dispersion of the liquid in the pressurized gas, the smaller the size of particle expected. Dukhin et al.,[14] after a complex mathematical treatment, were able to approximate this velocity according to the following expression:

$$u_c^{SS} = 29 \times \sqrt{\frac{\sigma}{\rho_g d_n}}\ (\text{cm s}) \quad (5)$$

Therefore, the effects of the physicochemical properties of the fluids involved in the process (density, viscosity, and interfacial tension) and the effect of the velocity of the jet on the mechanisms of jet disintegration, under specified operating conditions of the process (temperature, pressure, flow rate, orifice diameter) can be approximated by means of a dimensionless analysis.

3.2. Dimensional Analysis. The empirical equations proposed by Czerwonatis and Egger[9] were used, mainly to estimate the different disintegration regimes in the present study.

To calculate the dimensionless numbers Z^{**} and Re_L, estimations and experimental determinations have been made of the physicochemical properties required of the pure components involved in the process, NMP and CO_2. The influence of the concentration of ampicillin in NMP and the quantity of antisolvent that diffuses to the liquid phase before the disintegration of the jet occurs, have been ignored. In the same way, Chaves et al.[15] stated that only a negligible quantity of antisolvent diffuses to the liquid phase during the period of disintegration of the liquid jet.

One of the physicochemical properties that has more influence on the hydrodynamics of the system is the interfacial tension (σ). In fact, Dukhin et al., apart from the mode known as equilibrium interfacial tension (σ_{eq}), whose value is zero "in the region of a single phase" above MCP, proved the existence of a dynamic interfacial tension (DIT); as a consequence, despite being above supercritical conditions of complete miscibility, a gradient of density (isothermal DIT) and/or of temperature (nonisothermal DIT) between the phases in the initial instant of contact, this will give rise to a positive value of interfacial tension that stabilizes the jet against aerodynamic perturbations.[14]

Therefore, in the present analysis, two means will be used to determine the interfacial tension: one is the experimental determination of the equilibrium interfacial tension up to the point when the MCP is reached; the other is the estimation of the isothermal DIT at time zero ($\sigma_{t=0}$) above the MCP, which is the interfacial tension at the initial instant when the two phases come into contact with each other but without any diffusion between them occurring.

3.3. Thermodynamic Properties of Pure Substances at Elevated Pressures. 3.3.1. Density. The values of the densities of CO_2 under the pressure and temperature conditions that have been studied were obtained from the *Encyclopaedia of Gas*. However, since the effect of the temperature and pressure on the density of NMP is extremely small,[16] a constant value of the density of NMP, 1030 kg/m^3 (298 K and 1 bar), will be utilized for the calculations (Sigma−Aldrich).

3.3.2. Viscosity. The influence of the operating pressure on the viscosity of the liquid has been estimated using the equation proposed by Lucas:[17]

$$\frac{\mu}{\mu_{SL}} = \frac{1 + D(\Delta P_r/2.118)^A}{1 + Cw\Delta P_r} \quad (6)$$

where $\Delta P_r = (P - P_v)/P_c$. The values of μ_{SL} at the operating temperatures have been interpolated from experimental results found in the bibliography,[18] while the value of P_v (<1 bar) has been considered to be negligible. On the other hand, the viscosity of CO_2 has been obtained from the *Encyclopaedia of Gas*.

3.3.3. Dynamic Interfacial Tension. The dynamic interfacial tension at time zero ($\sigma_{t=0}$) was estimated using the equation of the Macleod−Sugden correlation (the Parachor parameter equation), which is widely utilized in the estimation of the disintegration regimes of the jet under supercritical conditions, considering that there is no diffusion between the phases at the initial instant of contact between them:[14,19]

$$\sigma_{t=0}^{1/4} = \sum_{i=1,\ldots,n}^{n} [P_i](\rho_l x_i - \rho_g y_i) \quad (7)$$

where x_i is the mole fraction of component i in the liquid phase and y_i is the mole fraction of component i in the vapor phase. The Parachor parameter for each component ($[P_i]$) has been obtained from the general data of contribution of groups,[17] obtaining the values $[P_{CO_2}] = 86.8$ and $[P_{NMP}] = 243.9$ as the result.

4. Results

4.1. Equilibrium Interfacial Tension. In Figure 4, the results obtained for the interfacial tension are listed for temperatures of 308, 313, and 328 K. Since the real mixture densities that resulted from mutual solubility are not known, the experimental density values for the pure components were used.

In case the density difference must be corrected after the experiments, the old σ_{eq} value must be divided by the old density difference. The resulting density-related value is then multiplied by the new (and improved) density difference.

At atmospheric pressure, the surface tension decreases as the temperature increases, which is thermodynamically proven. At increased pressure, σ_{eq} is dependent on mutual solubility, which, in turn, usually decreases as the temperature increases. As a result, the thermodynamic effect on σ_{eq} is compensated, leading to a point of inversion of the σ_{eq} isotherms.

At increased pressure, the interfacial tension decreases, because of increased mutual solubility. At 313 K, the σ_{eq} vanishes at ~100 bar, because of complete miscibility. Increasing the temperature to 328 K shifts this critical mixing point above 100 bar, enabling stable droplets at 100 bar to be generated. The course of σ indicates a critical mixing point of ~120 bar at 55 °C. On the other hand, it is not possible to obtain stable droplets at 308 K above 60 bar, because σ_{eq} becomes too small. The value of 308 K is near the critical temperature of CO_2, at which there is a sharp change in density at ~70 bar, coinciding with complete miscibility of the mixture under these conditions.

4.2. Estimated Regimes of Jet Disintegration at Elevated CO_2 Pressure. Table 1 gives the data for a series of 14 ampicillin precipitation experiments using the SAS process; for each experiment, there is an estimate of the type of disintegration regime when the NMP liquid solvent is injected by nebulizers with an orifice diameter of either 100 or 200 μm in a continuous-flow chamber of CO_2 at high pressure. The operating conditions that influence the hydrodynamics of the system, particularly the pressure, temperature, and flow rates of liquid solution, have been varied in the following ranges: $P = 80-180$ bar, $T = 308-328$ K, and $Q_L = 1-5$ mL/min. The combinations of these parameters represent conditions below, around, and above the MCP of the NMP−CO_2 system, in which all the possible disintegration regimes for a laminar jet have been estimated, as can be seen in Figure 5.

In addition, the transition from the sine wave breakup regime to the atomization regime has been contrasted with the critical jet velocity (the velocity at which the transition to atomization occurs) estimated from the empirical equation given by Dukhin et al.[14] As can be seen in Table 1, there is agreement between the estimates of this transition obtained using the two correlations, since, for those experiments in which an atomization regime is predicted, the velocity of the liquid jet exceeds or is of the same order as the critical velocity estimated.

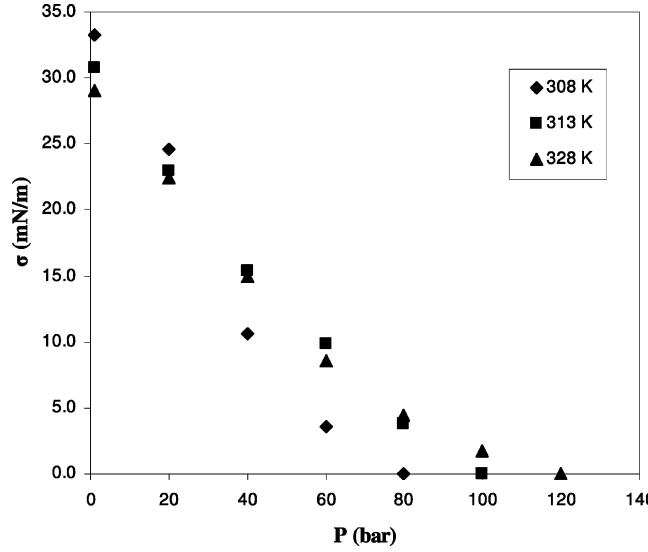

Figure 4. Interfacial tension as a function of pressure at different temperatures: (◆) 308 K, (■) 313 K, and (▲) 328 K.

In experiments 1, 2, 3, and 4, the solution of ampicillin in NMP has been injected within the continuous phase of SC CO_2 at pressures of 80, 100, 125, and 150 bar, respectively, with the remaining variables being held constant. At $P = 80$ bar, it has been estimated that the jet of the liquid solution disintegrates, according to a regime at the limit between Rayleigh breakup and sine wave breakup. As the pressure is increased, it is estimated that the liquid jet begins to become destabilized, principally by a decrease of the interfacial tension and a considerable increase of the density of the CO_2; then, the jet disintegrates according to a sine wave breakup regime, until the atomization regime is predicted at the pressure of 150 bar.

In experiments 5−10, NMP solutions have been injected, utilizing different combinations of orifice diameter and liquid solution flow rates, resulting definitively in different mean velocities of the liquid jet (v_L) for the same pressure and temperature conditions. As can be estimated in Figure 5, this velocity has extremely important influence, since a moment arrives when the force of inertia overcomes the capillary forces and the jet is destabilized; in consequence, transitions are expected from Rayleigh/sine wave breakup regimes (experiments 5, 7, and 9) to the atomization of the liquid (experiments 6, 8, and 10).

Lastly, in the remaining experiments, a more exhaustive study has been made of the influence of the liquid jet velocity, setting temperature, and pressure conditions that are found to be more favorable for the satisfactory precipitation of ampicillin.[8] In Table 1 and Figure 5, it can be observed that the jet of NMP may disintegrate passing through all the possible regimes, as a consequence of the increase in the velocity of the jet from 0.5 m/s to 2.6 m/s. Therefore, it is estimated that it is necessary to apply a flow rate of ~3 mL/min, equivalent to a velocity of ~1.6 m/s, to achieve the atomization of the liquid solution of NMP under the following conditions: $P = 180$ bar; $T = 328$ K; and utilizing an orifice diameter of $\varnothing_n = 200$ μm.

4.3. Interpretation of the Results. In previous studies of ampicillin precipitation by the SAS process,[7,8] it has been proven that a relationship exists between the macrostructure (physical appearance, qualitative characterization) and the microstructure (form and sizes of the particles, qualitative and quantitative characterization) of the precipitate obtained. Hence, two differentiated types of morphology can be identified: spherical nanoparticles of ampicillin that are obtained from a fine

Table 1. Estimated Regimes of NMP Jet Disintegration in Pressurized CO_2 as a Function of Different Pressure, Temperatures, Liquid Flow Rates, and Nozzle Diameters[a]

run number	$Ø_n$ (μm)	Q_L (mL/min)	v_L (m/s)	P (bar)	T (K)	$\sigma_{t=0}$ (mN/m)	$v_{critical}$ (m/s)	Re_L	Z^{**}	regimes of jet disintegration
1	100	1	2.1	80	313	3.8[b]	10.6	155	3.2	Rayleigh−sinuous
2	100	1	2.1	100	313	1.7	5	153	7.1	sinuous wave
3	100	1	2.1	125	313	0.7	2.9	151	18	sinuous−atomization
4	100	1	2.1	150	313	0.4	2.1	149	32	atomization
5	200	1	0.5	90	308	1.5	3.2	70	2.4	Rayleigh breakup
6	100	5	10.6	90	308	1.5	4.6	697	49	atomization
7	100	1	2.1	90	328	2.7[b]	9.3	184	3.3	sinuous wave
8	200	5	2.6	90	328	2.7[b]	6.6	460	4.2	sinuous−atomization
9	200	1	0.5	180	308	0.1	0.9	66	23	sinuous wave
10	100	5	10.6	180	308	0.1	1.2	661	465	atomization
11	200	1	0.5	180	328	0.6	2	87	4	Rayleigh−sinuous
12	200	2	1	180	328	0.6	2	174	8	sinuous wave
13	200	3	1.6	180	328	0.6	2	261	12	atomization
14	200	5	2.6	180	328	0.6	2	435	20	atomization

[a] Legend of symbols: $Ø_n$, orifice diameter; v_L, liquid jet velocity; P, pressure; T, temperature; $\sigma_{t=0}$, zero-time dynamic interfacial tension; $v_{critical}$, critical flow velocity; Re_L, Reynolds number of the liquid jet; and Z^{**}, a dimensionless number that describes the destabilizing effect of increased velocity on the external surface of the jet (see text). [b] Equilibrium interfacial tension.

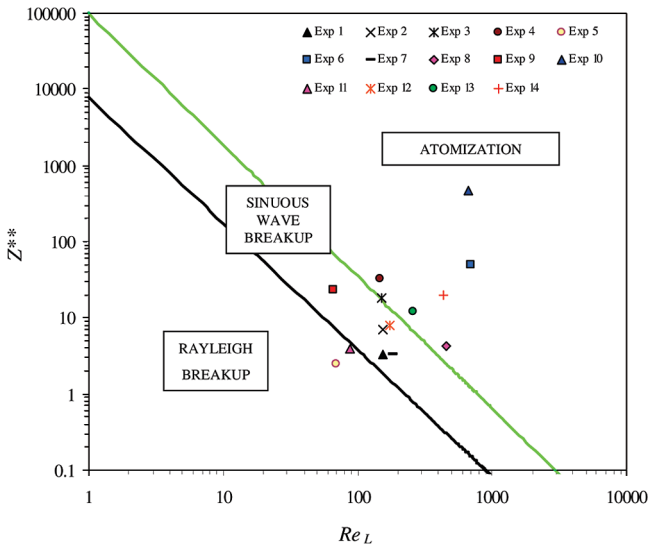

Figure 5. Approach to NMP jet disintegration in pressurized CO_2; the dark line determines the boundary between Rayleigh breakup and sinuous wave breakup regime, and the green line determines the boundary between the sinuous wave and atomization regimens.

precipitate with foamy texture, and particles of ampicillin with irregular forms and of larger size, which are characteristic of the precipitate formed by aggregates, compact films, and rods.

The macrostructure of the ampicillin precipitate obtained in each of the 14 experiments selected in the present article is described in Table 2. In the cases in which a fine precipitate constituted by spherical nanoparticles of ampicillin has been obtained, the range of the mean particle size (d_{50}) was 100−300 nm, with a coefficient of variation (CV) of ∼0.4. Therefore, in the present article, beyond establishing a correlation between the mean size of the nanoparticles and the hydrodynamic conditions of the process, the object is to explain, from the estimation of the different disintegration regimes as a function of the physicochemical properties and of the velocity of the jet, the two different morphologies obtained in the ampicillin precipitation experiments for a specific range of operating conditions. Thus, it will be possible to predict the limiting hydrodynamic conditions for the success of the test; in other words, it should be possible to specify the hydrodynamic conditions for orientating the process toward the formation of uniform spherical nanoparticles rather than irregular particles, of larger size, for a given solute−solvent−SC CO_2 system.

4.3.1. Effect of Operating Pressure. In the first of the cases (experiments 1, 2, 3, and 4), the effect of the pressure on the system's hydrodynamics, and its influence on the characteristics of the precipitate obtained, are analyzed. In Table 1 and Figure 5, it is estimated that an increase of the operating pressure from 80 bar to 150 bar may cause the dispersion of the liquid solution in the pressurized chamber starting from a regime close to that of Rayleigh, passing through the sine wave breakup until the atomization regime is reached. However, a change in the macroscopic morphology of the precipitate obtained only becomes evident for the change of pressure from 80 bar to 100 bar; that is, the morphology passes from a solid film obtained in the filter at a pressure of 80 bar, to a fine precipitate on the chamber walls and aggregates in the filter at pressures of 100−150 bar. Figure 6 shows the microstructure of the solid film obtained at 80 bar, where the mean size of particle was $d_{50} = 1.2$ μm and the coefficient of variation was CV = 0.7 μm; it also shows the fine precipitate produced at the pressures of 100, 125, and 150 bar, which is characterized by nanoparticles with a d_{50} value in the range of 100−300 nm and a CV value of ∼0.4.

The morphology of the precipitate obtained at a pressure of 80 bar, below the MCP_{313K} = 100 bar level (determined experimentally in the present work), is supposed to be in accordance with the Rayleigh regime estimated, since droplets with a diameter of approximately twice the diameter of the orifice would be produced;[19] then, because sufficient contact area would not be generated, the liquid phase does not evaporate in the dense phase of the CO_2. Instead, the liquid droplets accumulate in the filter, where the precipitate is obtained by the drying action of the CO_2. In contrast, for pressures of 100, 125, and 150 bar, from near the MCP_{313K} value to pressures considerably above this level, the presence of a precipitate occurring as aggregates in the filter may be explained by the existence of significant mechanisms that stabilize the liquid jet; the effect of these mechanisms would mean that, even when the equilibrium interfacial tension is zero, a definite interface would exist between the liquid jet (the entities or droplets that comprise the jet) and the dense gas. Therefore, the so-called "gaseous plume" or "gas-like jet", which is characteristic of states of complete miscibility of mixtures (above their MCP), would not be produced, even at pressures as high as the maximum tested in our study: 150 bar.

These important mechanisms of stabilization may be associated with the existence of the two modes of DIT established by Dukhin et al.[14] Apart from the isothermal DIT considered in

Table 2. Ampicillin Precipitated from NMP Jet Disintegration in Pressurized CO_2 as a Function of Different Pressure, Temperatures, Liquid Flow Rates, and Nozzle Diameters

run number	pressure, P (bar)	temperature, T (K)	liquid jet velocity, v_L (m/s)	macrostructure	regimes of jet disintegration
1	80	313	2.1	film of solid on the frit	Rayleigh−sinuous
2	100	313	2.1	fine precipitate on the wall and aggregate on the frit	sinuous wave
3	125	313	2.1	fine precipitate on the wall and aggregate on the frit	sinuous−atomization
4	150	313	2.1	fine precipitate on the wall and aggregate on the frit	atomization
5	90	308	0.5	small aggregates on the frit	Rayleigh breakup
6	90	308	10.6	fine precipitate on the wall and small aggregates, rods on the frit	atomization
7	90	328	2.1	aggregates impregnated with solvent on the frit	sinuous wave
8	90	328	2.6	small aggregates on the frit	sinuous−atomization
9	180	308	0.5	rods on the frit	sinuous wave
10	180	308	10.6	small aggregates on the frit	atomization
11	180	328	0.5	solvent on the wall and on the frit	Rayleigh−sinuous
12	180	328	1	fine precipitate on the wall and sticky precipitate on the frit	sinuous wave
13	180	328	1.6	fine precipitate on the wall and on the frit	atomization
14	180	328	2.6	fine precipitate on the wall and on the frit	atomization

the present study, which is due to a concentration gradient at the instant of contact of the two phases, the other mode, called "non-isothermal DIT" should be taken into account, because the transfer of matter occurs in association with the release or consumption of heat, as a consequence of the heat of solution or heat of evaporization (excess molar enthalpy). This implies that the temperature of the jet (T_j) may be different from the temperature of the precipitation cell (T_c); this difference (ΔT_j), and its sign, are influenced by many factors—principally, by the operating pressure and temperature—and the difference varies for different solvent−antisolvent combinations. For the NMP−SC CO_2 combination, the excess molar enthalpies are exothermal, and researchers have measured significant positive temperature gradients of 6.2 K, 4.2 K, and 3.9 K for an operating temperature of 313 K and pressures of 95, 150, and 200 bar, respectively.[20] Note that nonisothermal DIT is defined based on a local equilibrium at the temperature reached in the sublayer of the liquid jet adjacent to the dense medium ($T_c + \Delta T_j$). This implies that the $MCP_{T_c=313K+\Delta T_j}$ is higher than the $MCP_{T_c=313K}$; this would therefore explain why, at a pressure of 100 bar, close to the $MCP_{T_c=313K}$ value, the sublayer of the liquid jet may be in a subcritical state (immiscibility) while the precipitation cell may be in a critical or even supercritical state (complete miscibility).

Taking these considerations into account, at a pressure of 100 bar, there would be agreement between the morphologies obtained and the regime of sine wave breakup estimated. In this type of dispersion, it is well-known that polydisperse droplets are produced; then, as the smaller droplets fall, they are dissolved in the dense medium,[14] which would be the source of the fraction of fine precipitate obtained, whereas the droplets of larger size that would accumulate at the bottom of the chamber form the solid aggregates that have been mentioned.

For pressures of 125 and 150 bar, that is, considerably above the MCP_{313K} value, both DIT modes would be enormously reduced,[14] and therefore the associated mechanisms of stabilization would be of a different nature. In these cases, the stabilization could be explained by the presence of the ampicillin (concentration of the solution: 20 mg/mL) which would modify the equilibrium of the binary NMP−CO_2 system in such a way that the pressure at which the NMP and CO_2 achieve complete miscibility at 313 K (MCP_{313K}) would be increased enormously.[21] According to this assumption, conditions would be those of immiscibility with an interfacial tension much greater than that considered in the present study; that is, with Z^{**} values less than those estimated. In consequence, the liquid solution would not reach the stage of being atomized under the operating conditions studied: rather, it would disintegrate, according to a sine wave breakup regime, and create a precipitate of the same characteristics as that obtained at 100 bar.

Therefore, from all the above hypotheses, it seems that the effects of the increase of pressure under the operating conditions studied (the reduction of σ_{eq} and the increase in the density of the CO_2) are not sufficiently large to overcome the various stabilization mechanisms mentioned. Consequently, it is thought that the liquid jet forms a dispersion that is not sufficiently fine

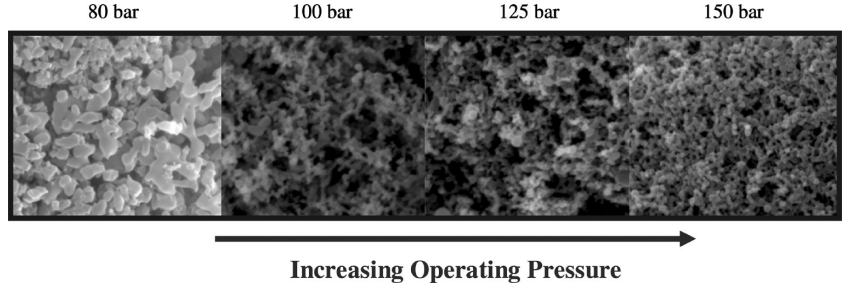

Figure 6. Effect of operating pressure on microstructure of ampicillin powder obtained by the SAS experiments performed at 80, 100, 125, and 150 bar, keeping the other operating conditions constant.

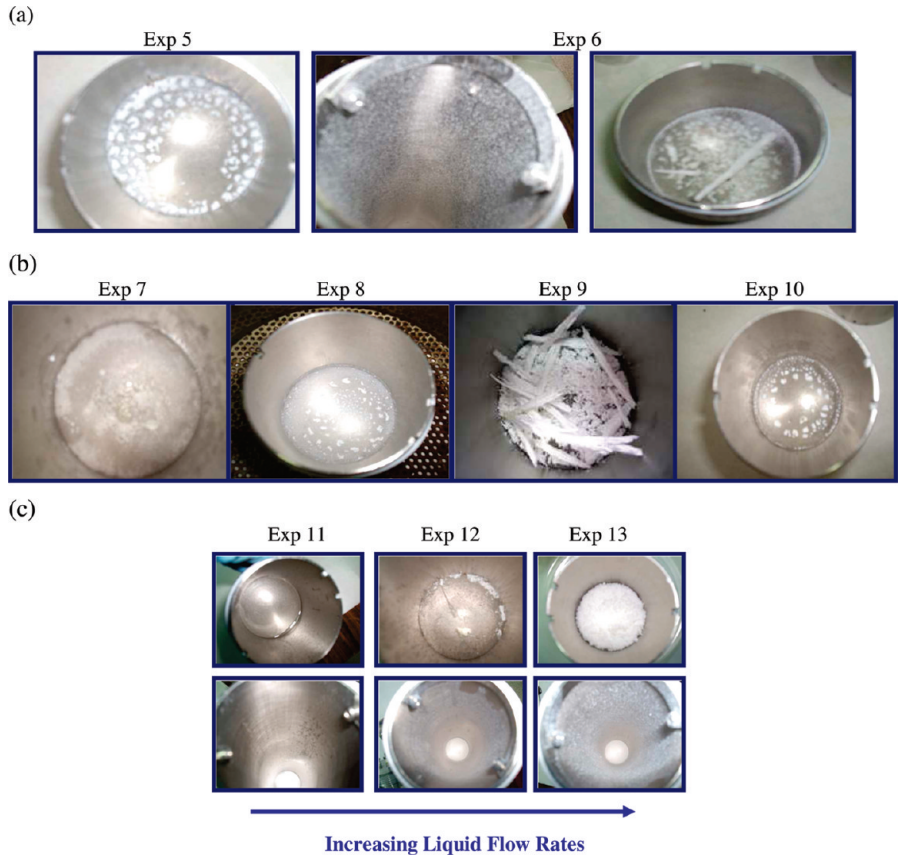

Figure 7. Macrostructure of ampicillin powder produced by SAS experiments: (a) experiments 5 and 6 with jet velocities of 0.5 and 10.6 m/s at 90 bar and 308 K, respectively; (b) experiments 7, 8, 9, and 10, with jet velocities of 2.1 m/s, 2.6 m/s, 0.5 m/s, and 10.6 m/s, respectively, at the operating pressures and temperatures of 90 bar and 328 K for experiments 7 and 8 and 180 bar and 308 K in experiments 9 and 10; and (c) experiments 11, 12, and 13 with a jet velocity of 0.5 m/s, 1 m/s, and 1.6 m/s, respectively (at 180 bar, 328 K, and 200 μm).

and uniform to accelerate the transfer of matter between the phases, to evaporate all the NMP in the dense phase of the CO_2, and to generate constant levels of supersaturation that would lead to the production of a homogeneous precipitate consisting of spherical nanoparticles of ampicillin.

4.3.2. Effect of the Jet Velocity. The objective in experiments 5, 6, 7, 8, 9, and 10 is to analyze the influence of the mean velocity of the jet of liquid solution (v_L); the experiments explore the influence of different orifice diameters and solution flow rates at different conditions of pressure and temperature on the morphological characteristics of the precipitate obtained. The transitions from Rayleigh (experiment 5) and sine wave (experiments 7 and 9) breakup regimes to atomization of the liquid (experiments 6, 8, and 10) as the mean velocity of the jet is increased are shown in Table 1 and Figure 5.

In experiments 5 and 6, an important change occurs in the morphologies of the precipitates obtained that may be related to the transition of the disintegration regime estimated; as can be seen in Figure 7, the form of the precipitate obtained passes from small aggregates collected in the filter, forming concentric circles, to a fine precipitate deposited in larger quantities on the walls of the chamber, as well as small aggregates and rods in the filter.

The morphologies of the precipitates obtained in experiments 5 and 6, under the operating conditions near or above the MCP_{308K} (80 bar), again may be explained by the influence of the DIT modes previously discussed (isothermal DIT and nonisothermal DIT) that stabilize the liquid jet in contact with the dense phase and prevent it from disintegrating in the form of a "gas-like jet". Thus, the morphology of the precipitate from experiment 5 may be due to the estimated Rayleigh regime, since the precipitation would have only occurred in the liquid phase that accumulated in the filter, after its dispersion into droplets with a size of approximately twice the diameter of the orifice. In experiment 6, the considerable increase of the jet velocity may overcome (by force of inertia) the stabilization mechanisms of the isothermal and nonisothermal DIT; however, this would not be high enough to overcome the stabilization mechanism associated with the presence of ampicillin (at 100 mg/mL). Thus, the liquid solution would not be completely atomized, as had been estimated; instead, it would disintegrate in accordance with a sine wave breakup regime, resulting in the two types of morphologies that have been obtained.

Experiments 5 and 6 emphasize the importance of the hydrodynamics in the SAS process: for the same pressure and temperature conditions, the effect of an increase of the jet velocity is to direct the process toward the formation of spherical nanoparticles of ampicillin in place of solid aggregates constituted by irregular- and larger-size particles; consequently, the output of the process also increases.

In experiments 7−10, the transition to the atomization regime by the increase of the velocity of the jet does not result, in either case, in the production of precipitates with morphologies similar to those previously obtained for the same regimes. As shown in Figure 7, in the four experiments, the only precipitate obtained is that formed in the filter by solid aggregates with different forms: solid film, concentric circles, and rods. Therefore, these represent cases that demonstrate the great complexity of the SAS process; in this process, factors such as the ternary phase equilibrium, matter transfer between the phases, and the kinetics of nucleation and growth will need to be considered, in addition to the limiting hydrodynamic conditions.

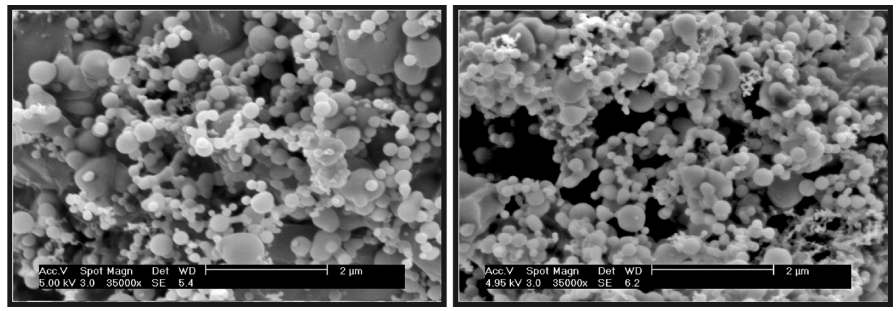

Figure 8. Micrographs showing the microstructure of the ampicillin powder obtained by SAS experiment 14 with a jet velocity of 2.6 m/s (at 180 bar, 328 K, and 200 μm).

This last finding means that there is a need for more-precise study of the influence of the velocity of the liquid jet in the SAS process. To do this, experiments 11−14 were conducted. In these experiments, the velocity of the jet has been varied over the range of 0.5−2.6 m/s, using an orifice diameter of 200 μm and under the pressure and temperature conditions found to be most favorable for obtaining a homogeneous precipitate of spherical nanoparticles of ampicillin.[8] Figure 8 shows the microstructure of the precipitate obtained in experiment 14, conducted at the conditions mentioned (180 bar and 328 K).

Table 1 and Figure 5 show that increasing the liquid solution flow rate from 1 mL/min to 5 mL/min causes the jet to disintegrate, passing through the three possible regimes: Rayleigh (experiment 11), sine wave breakup (experiment 12), and atomization (experiments 13 and 14). The pressure conditions under which the experiments have been conducted are considerably higher than the MCP_{328K} value (120 bar); however, in some of the tests, the presence of remains of solvent and precipitates in the filter may be explained again by the modification of the phase equilibrium of the binary NMP−CO_2 system, because of the presence of the ampicillin (at 60 mg/mL).

The lowest flow rate tested (1 mL/min, in experiment 11), which is equivalent to a jet velocity of 0.5 m/s ($\text{Ø}_n = 200$ μm), led to an unsatisfactory test result, which may be in agreement with the Rayleigh-type regime estimated; this is because the droplets that formed would not generate sufficient contact area to produce saturation while they are in motion, and, consequently, ampicillin is not precipitated. As can be seen in Figure 7, the liquid seems to be dispersed both on the walls and accumulated in the filter.

For experiment 12, in which the flow rate is increased to 2 mL/min (that is, to a jet velocity of 1 m/s), a dispersion of the sine wave breakup type is estimated. Considering that a polydisperse distribution of droplets is produced in this regime, it is very well correlated with the experimental results obtained; as can be seen in Figure 7, an appreciable quantity of fine precipitate on the walls is obtained and this would have originated from the finer droplets of the distribution, while the small aggregates of precipitate with sticky texture in the filter are indicative of the accumulation of droplets of larger size.

In experiment 13, in which there is an increase of the liquid flow rate to 3 mL/min ($v_L = 1.6$ m/s), it is estimated that the transition is complete, and the liquid is atomized. Therefore, as can be observed in Figure 7, the large quantity of fine precipitate with foamy texture obtained both on the walls and accumulated in the filter (characteristic of nanoparticles) would have originated from the fully atomized and homogeneous dispersion that is occurring in the precipitation chamber. Finally, the last experiment—experiment 14—was performed with a further increase of the liquid flow rate to 5 mL/min ($v_L = 2.6$ m/s). In this experiment, a satisfactory precipitation of ampicillin is obtained, similar to that obtained in experiment 13; again, this would be in accordance with the estimated atomization regime.

5. Conclusions

The application of the empirical hydrodynamics model has allowed the estimate of the disintegration regimes for each ampicillin precipitation experiment, considering the operating conditions that influence the hydrodynamics of the system, particularly the pressure, temperature, and flow rates of the liquid solution.

The morphologies of the ampicillin precipitates obtained when the operating pressure is below the critical point of the mixture (MCP) at the operating temperature can be explained from applying the empirical model. However, it is proposed that important stabilization mechanisms explain the morphologies of the ampicillin precipitates obtained when the operating pressure was near and even considerably above the MCP at the operating temperature.

The results from the application of the empirical model cannot explain the morphologies of the precipitates obtained in experiments 7−10. Therefore, these represent cases that demonstrate the great complexity of the SAS process; in this process, factors such as the ternary phase equilibrium, matter transfer between the phases, and the kinetics of nucleation and growth will need to be considered, in addition to the limiting hydrodynamic conditions.

Finally, in experiments 11−14, the morphologies of the precipitates obtained were closely correlated with each estimated disintegration regime. These results highlight the fact that there are limiting hydrodynamic conditions that must be overcome to achieve a dispersion of the liquid solution in the dense medium; this dispersion must be sufficiently fine and homogeneous to direct the process toward the formation of uniform spherical nanoparticles and to the achievement of higher yields.

Acknowledgment

We are grateful to the Spanish Ministry of Science and Technology (Project No. PPQ2003-04245) for financial support. We also express our gratitude to the laboratory of EUROTECHNICA Ingenieurbüro GmbH (Bargteheide, Germany), for the measurements of interfacial tensions.

Nomenclature

Parameters

A, C, and D = constants that are dependent on the reduced temperature T_r

C_d = coefficient of discharge

d_{50} = mean particle size

Ø_n = orifice diameter

Oh = jet Ohnesorge number; $Oh = (We_l)^{1/2}/(Re_l) = \mu_l/(\sigma\rho_l d_n)^{1/2}$
$[P_i]$ = parachor parameter of component i
P = operating pressure (Pa)
P_v = vapor pressure (Pa)
Re_L = jet Reynolds number, ratio of inertial force to viscous force; $Re_L = \rho_l v_l d_n/\mu_l$
T_c = critical temperature
T_r = reduced temperature; $T_r = T/T_c$
u_c^{SS} = critical jet velocity (m/s)
v_g = gas jet velocity (m/s)
v_l = liquid jet velocity (m/s)
w = acentric factor
We_g = gas jet Weber number, ratio of inertial force to superficial force; $We_g = (\rho_g v_g^2 d_n)/\sigma$
Z^* = modified dimensionless number; $Z^* = Oh_l(We_g)^{1/2} = (\eta_l v/\sigma)(\rho_g/\rho_l)^{1/2}$
Z^{**} = modified dimensionless number; $Z^{**} = Z^*(\mu_l/\mu_g)^{1/2} = (\mu_l v/\sigma)(\rho_g/\rho_l)^{1/2}(\mu_l/\mu_g)^{1/2}$

Greek Symbols

ρ_g = density of the gas phase (kg/m^3)
ρ_l = density of the liquid phase (kg/m^3)
ρ_n = nozzle diameter (m)
μ = viscosity of the liquid at operating pressure P (cP)
μ_g = hydrodynamic viscosity of the gas phase (Pa s)
μ_l = hydrodynamic viscosity of the liquid phase (Pa s)
μ_{SL} = viscosity of the saturated liquid at vapor pressure P_v (Pa s)
σ_{eq} = equilibrium interfacial tension (N/m)
$\sigma_{t=0}$ = zero-time dynamic interfacial tension DIT (N/m)

Abbreviations

DIT = dynamic interfacial tension (N/m)
MCP = critical point of the mixture
NMP = *N*-methyl-pyrrolidone
SC CO_2 = supercritical carbon dioxide

Literature Cited

(1) Won, D.-H.; Kim, M.-S.; Lee, S.; Park, J.-S.; Hwang, S.-J. Improved physicochemical characteristics of felodipine solid dispersion particles by supercritical anti-solvent precipitation process. *Int. J. Pharm.* **2005**, *301*, 199.

(2) Van Nijlen, T.; Van Den Mooter, G.; Kinget, R.; Augustijns, P.; Blaton, N.; Brennan, K. Improvement of the dissolution rate of artemisinin by means of supercritical fluid technology and solid dispersions. *Int. J. Pharm.* **2003**, *254*, 173.

(3) Reverchon, E.; Della Porta, G.; Spada, A.; Antonacci, A. Griseofulvin micronization and dissolution rate improvement by supercritical assisted atomization. *J. Pharm. Pharmacol.* **2004**, *56*, 1379.

(4) Martin, A.; Cocero, M. J. Numerical modeling of jet hydrodynamics, mass transfer, and crystallization kinetics in the supercritical antisolvent (SAS) process. *J. Supercrit. Fluids* **2004**, *32*, 203.

(5) Lora, M.; Bertucco, A.; Kikic, I. Simulation of the semicontinuous supercritical antisolvent recrystallization process. *Ind. Eng. Chem. Res.* **2000**, *39*, 1487.

(6) Dukhin, S. S.; Shen, Y.; Dave, R.; Pfeffer, R. Droplet mass transfer, intradroplet nucleation and submicron particle production in two-phase flow of solvent-supercritical antisolvent emulsion. *Colloids Surf. A* **2005**, *261*, 163.

(7) Tenorio, A.; Gordillo, M. D.; Pereyra, C.; de la Ossa, E. J. M. Controlled submicroparticle formation of ampicillin by supercritical antisolvent precipitation. *J. Supercrit. Fluids* **2007**, *40*, 308.

(8) Tenorio, A.; Gordillo, M. D.; Pereyra, C. M.; de la Ossa, E. J. M. Relative Importance of the Operating Conditions Involved in the Formation of Nanoparticles of Ampicillin by Supercritical Antisolvent Precipitation. *Ind. Eng. Chem. Res.* **2007**, *46*, 114.

(9) Czerwonatis, N.; Eggers, R. Disintegration of Liquid Jets and Drop Drag Coefficients in Pressurized Nitrogen and Carbon Dioxide. *Chem. Ing. Tech.* **2000**, *72*, 1371.

(10) Andreas, J. M.; Tucker, W. B. Boundary Tension by Pendant Drop. *J. Phys. Chem.* **1938**, *42*, 1001.

(11) Jaeger, Ph T.; Schnitzler, J. V.; Eggers, R. Interfacial Tension of Fluid Systems Considering the Non-Stationary Case with Respect to Mass Transfer. *Chem. Eng. Technol.* **1996**, *19*, 197.

(12) Song, B.; Springer, J. Determination of Interfacial Tension from the Profile of a Pendant Drop Using Computer-Aided Image Processing. 1. Theoretical. *J. Colloid Interface Sci.* **1996**, *184*, 64.

(13) Lefebvre, A. H. *Atomization and Sprays*; Hemisphere Publishing Corp.: New York, 1989.

(14) Dukhin, S. S.; Zhu, C.; Dave, R.; Pfeffer, R.; Luo, J. J.; Chavez, F.; Shen, Y. Dynamic interfacial tension near critical point of a solvent−antisolvent mixture and laminar jet stabilization. *Colloids Surf. A* **2003**, *229*, 181.

(15) Chávez, F.; Debenedetti, P. G.; Luo, J. J.; Dave, R. N.; Pfeffer, R. Estimation of the characteristic time scales in the supercritical antisolvent process. *Ind. Eng. Chem. Res.* **2003**, *42*, 3156.

(16) Salmon, J. Physical Properties of *N*-Methylpyrrolidinone as Functions of Temperature. *J. Chem. Eng. Data* **1987**, *32*, 422.

(17) Bruce, E.; Poling, J. M. P.; O'Connell, J. *The Properties of Gases and Liquids*; McGraw−Hill: New York, 2000.

(18) Amr Henni, J. J. H.; Tontiwachwuthikul, P.; Chakma, A. Volumetric Properties and Viscosities for Aqueous *N*-Methyl-2-pyrrolidone Solutions from 25 to 70 °C. *J. Chem. Eng. Data* **2004**, *49*, 231.

(19) Badens, E.; Boutin, O.; Charbit, G. Laminar jet dispersion and jet atomization in pressurized carbon dioxide. *J. Supercrit. Fluids* **2005**, *36*, 81.

(20) María, J.; Davila, A. C.; Pando, C. Excess molar enthalpies for binary mixtures related to supercritical antisolvent precipitation: Carbon dioxide + *N*-methyl-2-pyrrolidone. *J. Supercrit. Fluids* **2007**, *42*, 172.

(21) Reverchon, E.; Caputo, G.; DeMarco, I. Role of Phase Behavior and Atomization in the Supercritical Antisolvent Precipitation. *Ind. Eng. Chem. Res.* **2003**, *42*, 6406.

Received for review December 17, 2008
Revised manuscript received June 23, 2009
Accepted June 30, 2009

IE801940P